

Tuning impurity states in bilayer graphene.

Hari P. Dahal,^{1,2} A. V. Balatsky,^{2,3} and Jian-Xin Zhu^{2,*}

¹*Department of Physics, Boston College, Chestnut Hill, MA, 02467*

²*Theoretical Division, Los Alamos National Laboratory, Los Alamos, New Mexico 87545*

³*Center for Integrated Nanotechnology, Los Alamos National Laboratory, Los Alamos, New Mexico 87545*

We study the impurity states in bilayer graphene in the unitary limit using Green's function method. Unlike in single layer graphene, the presence of impurities at two non-equivalent sites in bilayer graphene produce different impurity states which is understood as the change in the band structure due to interlayer hopping of electrons. The impurity states can also be tuned by changing the band structure of bilayer graphene through external electric field bias.

PACS numbers:

I. INTRODUCTION

In recent years, the fabrication of few layers of graphene systems^{1,2,3} has attracted a lot of attention to study the electronic properties of these systems. The electrons in single graphene show some unconventional electronic properties such as the half integer quantum Hall effect, and Klein paradox. The electrons in bilayer systems also show some interesting properties as seen in quantum Hall effect. Many properties of single and bilayer graphenes also differ because of the different crystal structure. In this communication we present a systematic study of impurity effects in bilayer graphene and contrast it with those of the single layer counterpart.

The fundamental difference between single and bilayer graphene originates from their crystal structure. Single layer graphene is an atomically thin two-dimensional hexagonal packing of sp^2 bonded carbon atoms. It is the building block of (multi-layer) graphene. One unit cell of single layer graphene has two non-equivalent lattice sites (A, B). As a result, the electron wave function is spinor-like, where the sublattice index plays the role of pseudo-spin. The tight binding calculation⁴ shows that the electrons in single layer graphene disperse linearly, i.e. ($E_k = \pm v_F k$), where $v_F = \frac{3ta}{2} = 5.8 \text{ eV\AA}$ is the Fermi velocity, $t = 3.0 \text{ eV}$ is the nearest neighbor hopping energy in the plane, and a is the lattice constant, and hence are called the massless Dirac fermions. The bilayer graphene, as shown schematically in Fig. 1, can be thought of as a stacking of two identical single layer graphenes in the third dimension. In one of the common ways of layer stacking, known as Bernal stacking, only one of the non-equivalent lattice sites (site-A) stay on top of each other, another site (B) lies in the middle of the hexagon of the other layer.⁵ The electron can hop between the layers along the bonding of these two A-sites with a hopping energy (t_\perp), which is about ten times smaller than the hopping energy along the plane. This interlayer hopping hybridizes the p_z orbital of the carbon atom at site-A resulting in different dispersion relation of the electrons, ($E_k = \pm \frac{t_\perp}{2} \pm \sqrt{\frac{t_\perp^2}{4} + v_F^2 k^2}$).^{6,7,8} Two of the branches of the electronic band touch each other at the Fermi energy, whereas the other two branches be-

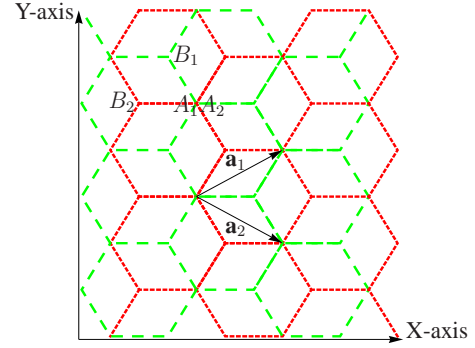


FIG. 1: (Color online) Lattice structure of bilayer graphene under consideration for a tight binding calculation. The green (dashed) line forms the top layer and the red (dotted) line forms the bottom layer.

come gapped with energy gap equal to t_\perp . The dispersion relation of the electrons corresponding to the gapless branches can be expressed in parabolic form at low momenta. The electron energy in this case have parabolic dispersion at low momenta. In addition to this difference of the band structure between single and bilayer graphenes, the bilayer system gives a freedom of tailoring the band structure by applying an external electric field bias (V) on the two layers. The dispersion relation in the presence of the external field bias becomes,^{8,9}

$$E_K = \pm \sqrt{\frac{V^2}{4} + \frac{t_\perp^2}{2} + v_F^2 k^2} \pm \sqrt{\frac{t_\perp^4}{4} + (V^2 + t_\perp^2) v_F^2 k^2}, \quad (1)$$

which shows that the two valence (conduction) bands shift below (above) the Fermi energy by $V/2$.

To understand the electronic property of these systems, it is important to study the revealing impurity effects. The impurity states in single layer graphene has been studied by Wehling *et al.*¹⁰ and by Bena.¹¹ It has been shown that if an impurity is introduced on a lattice site, a virtually bound impurity resonance state can be induced, which can be seen as an enhancement of the local density of states (LDOS) at the neighboring site. This effect is symmetric with respect to the sublattice the impurity is on, i.e., an impurity at site B shows exactly the

same effect as it is at site A. In bilayer graphene, due to the bonding between the sites A of the two layers, the site A and B in each layer are no longer equivalent. The interlayer hopping distinctly differentiates the two sites. So we expect to see different impurity states with respect to the location of the impurity. In addition, it is natural to expect that the external bias which changes the band structure also modifies the properties of the impurity states. This motivates us to study the impurity states in bilayer graphene as a function of both t_{\perp} and V . The impurity effect in single layer graphene is contained in our discussion as a special case of bilayer graphene where $t_{\perp} = 0$.

The outline of the paper is as follows: In Sec. II, we present a Green's function method to study the impurity effects. For the clean system, the results from the Green's function method is benchmarked with the exact diagonalization. In Sec. III, we present a systematic set of results and discussions. Concluding remarks are given in Sec. IV.

II. THEORETICAL METHOD

In this section we describe the theoretical method used to calculate the LDOS in the bilayer graphene

using Green's function. We need to find the form of the Hamiltonian to define the free particle Green's function. The Green's function in the presence of the impurity potential is obtained by using the Dyson's equation. We derive a tight binding Hamiltonian using the lattice structure of the bilayer graphene as shown in Fig. 1. The basis vectors are chosen to be, $a_1 = (\frac{3a}{2}, \frac{-\sqrt{3}a}{2})$, and $a_2 = (\frac{3a}{2}, \frac{\sqrt{3}a}{2})$. The corresponding basis vectors of the reciprocal space is given by $b_1 = (\frac{2\pi}{3a}, \frac{-2\pi}{\sqrt{3}a})$, and $b_2 = (\frac{2\pi}{3a}, \frac{2\pi}{\sqrt{3}a})$. Sites A_1 and A_2 are connected along the z -direction, the electrons have t_{\perp} hopping energy in this direction. We have assumed that the layer which has lattice sites A_1, B_1 is biased with $V/2$ and the layer which has lattice sites A_2, B_2 with $-V/2$ so that the potential difference between the two layers is V . For the convenience of discussion, these two layers are called the top and bottom layers, respectively.

The tight binding equations for this lattice structures in the clean case can be written as,

$$\frac{V}{2}\phi_{A_1} - t[2\exp(\frac{-ik_x a}{2})\cos(\frac{k_y a\sqrt{3}}{2}) + \exp(ik_x a)]\phi_{B_1} - t_{\perp}\phi_{A_2} = E\phi_{A_1}, \quad (2a)$$

$$-t[2\exp(\frac{ik_x a}{2})\cos(\frac{k_y a\sqrt{3}}{2}) + \exp(-ik_x a)]\phi_{A_1} + \frac{V}{2}\phi_{B_1} = E\phi_{B_1}, \quad (2b)$$

$$-t_{\perp}\phi_{A_1} + \frac{-V}{2}\phi_{A_2} - t[2\exp(\frac{ik_x a}{2})\cos(\frac{k_y a\sqrt{3}}{2}) + \exp(-ik_x a)]\phi_{B_2} = E\phi_{A_2}, \quad (2c)$$

$$-t[2\exp(\frac{-ik_x a}{2})\cos(\frac{k_y a\sqrt{3}}{2}) + \exp(ik_x a)]\phi_{A_2} + (\frac{-V}{2})\phi_{B_2} = E\phi_{B_2}. \quad (2d)$$

These equations can be written in a matrix form,

$$\hat{H}_{\mathbf{k}} \begin{pmatrix} \phi_{A_1} \\ \phi_{B_1} \\ \phi_{A_2} \\ \phi_{B_2} \end{pmatrix} = \varepsilon_n \begin{pmatrix} \phi_{A_1} \\ \phi_{B_1} \\ \phi_{A_2} \\ \phi_{B_2} \end{pmatrix}. \quad (3)$$

Here,

$$\hat{H}_{\mathbf{k}} = \begin{pmatrix} V/2 & \tilde{t} & -t_{\perp} & 0 \\ \tilde{t}^* & V/2 & 0 & 0 \\ -t_{\perp} & 0 & -V/2 & \tilde{t}^* \\ 0 & 0 & \tilde{t} & -V/2 \end{pmatrix}, \quad (4)$$

with $\tilde{t} = -t[2\exp(\frac{-ik_x a}{2})\cos(\frac{k_y a\sqrt{3}}{2}) + \exp(ik_x a)]$ and \tilde{t}^* is the complex conjugate of \tilde{t} .

The Green's function corresponding to this Hamiltonian

nian can be expressed as,

$$\hat{G}^{(0)}(\mathbf{k}, \omega) = [\omega \hat{1} - \hat{H}_{\mathbf{k}}]^{-1}, \quad (5)$$

where $\hat{1}$ represents the unit matrix. As long as all introduced impurities (up to 4) are located within a single cell, we can express the local Green's function exactly through the T-matrix method, which leads to

$$\hat{G}_{ij}(\omega) = \hat{G}_{ij}^{(0)}(\omega) + \hat{G}_{i0}^{(0)}(\omega) \hat{T}(\omega) G_{0j}^0(\omega). \quad (6)$$

Here the T-matrix $\hat{T}(\omega) = \hat{U}(1 - G^{(0)}(\omega) \hat{U})^{-1}$, the local Green's function $\hat{G}_{ij}^{(0)}(\omega) = \frac{1}{N} \sum_{\mathbf{k}} \hat{G}^{(0)}(\mathbf{k}, \omega)$ where the summation is over the first Brillouin zone, and \hat{U} is the matrix representation of the impurity potential. The local density of states at different sites is given by, $N_{A1} = \frac{-1}{\pi} G_{11}(\omega + i\gamma)$, $N_{B1} = \frac{-1}{\pi} G_{22}(\omega + i\gamma)$, $N_{A2} = \frac{-1}{\pi} G_{33}(\omega + i\gamma)$, $N_{B2} = \frac{-1}{\pi} G_{44}(\omega + i\gamma)$, where γ is the lifetime broadening. For numerical calculation all relevant energies are measured in terms of the intralayer hopping energy of the electron, t . For simplicity we use the impurity potential close to the unitary limit, $U = 100$. The number of 1024×1024 \mathbf{k} points are used in the Brillouin zone. The intrinsic lifetime broadening of $\gamma = 0.005$ is taken. When we present results, unless otherwise stated, the panel *a* to *d* represent the LDOS at sites A_1, B_1, A_2 , and B_2 , respectively. In each figure, the DOS is plotted (along the vertical axis) as a function of energy E (along the horizontal axis).

We can also calculate DOS in the absence of impurities using eigenvalues and eigenvectors of Hamiltonian matrix, Eq. (4). A little algebra yields the eigenvalues

$$\varepsilon_n = \mp \sqrt{\frac{V^2}{4} + \frac{t_{\perp}^2}{2} + \tilde{t}\tilde{t}^*} \mp \sqrt{\frac{t_{\perp}^4}{4} + (V^2 + t_{\perp}^2)\tilde{t}\tilde{t}^*}, \quad (7)$$

where ε_n represents the four eigenvalues. Note that the linearization of Eq. (7) near the corner of the Brillouin zone reduces to Eq. (1).

The corresponding eigenvectors are given by a general equation,

$$\begin{pmatrix} \phi_{A1, \varepsilon_n} \\ \phi_{B1, \varepsilon_n} \\ \phi_{A2, \varepsilon_n} \\ \phi_{B2, \varepsilon_n} \end{pmatrix} = \begin{pmatrix} |\tilde{t}|^2 - (\frac{V}{2} + \varepsilon_n)^2 \\ |\tilde{t}|^2(\varepsilon_n - \frac{V}{2}) + (\frac{V}{2} + \varepsilon_n)(t_{\perp}^2 + \frac{V^2}{4} - \varepsilon_n^2) \\ \frac{\frac{V}{2} + \varepsilon_n}{t} \\ 1 \end{pmatrix} \quad (8)$$

where substituting four different values of ε_n gives the four sets of eigenvectors. We normalize thus obtained 4×4 matrix of the eigenvectors and calculate the density of states on four nonequivalent sites using the standard equation,

$$N_{\alpha\beta}(E) = \frac{1}{N\pi} \sum_{\mathbf{k}, \varepsilon_n} |\phi_{\alpha\beta, \varepsilon_n}(\mathbf{k})|^2 \left[\frac{\gamma}{(E - \varepsilon_n)^2 + \gamma^2} \right], \quad (9)$$

where $\alpha = A, B$, $\beta = 1, 2$, $\phi_{\alpha\beta, \varepsilon_n}(\mathbf{k})$ is the normalized eigen-vectors. We used this DOS to check the result obtained by Green's functions method in the absence of impurity.

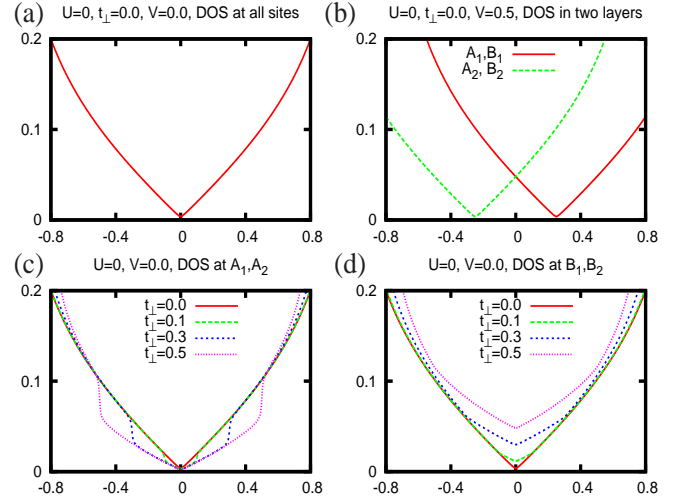


FIG. 2: (Color online) The density of states as a function of energy is shown. a) For $t_{\perp} = 0$ the DOS at all sites is equal, and vanishes linearly at the Fermi energy. b) For $t_{\perp} = 0$, and $V \neq 0$, the DOS curve for sites of the top (bottom) layer shifts above (below) the Fermi energy by $V/2$ creating finite DOS at the Fermi level. c) For $t_{\perp} \neq 0$ DOS at A sites of both layers is equal and for $-t_{\perp} < E < t_{\perp}$ it decreases compared to the single layer case. d) DOS at sites B of both layers is equal and for $-t_{\perp} < E < t_{\perp}$ it increases compared to the single layer case.

III. RESULTS AND DISCUSSIONS

A. Clean limit

Before getting in to the discussion of the impurity states, we first discuss the effects of V and t_{\perp} on the DOS in the absence of the impurity. For $V = 0$, and $t_{\perp} = 0$, the DOS at every sites is equal and it vanishes linearly in E close to the Fermi energy as shown in Fig. 2(a). For $t_{\perp} = 0$ but $V \neq 0$ the DOS in two layers is different. The overall variation of the DOS is still preserved but the DOS curve of upper (lower) layer shifts towards positive (negative) energy region by $V/2$, Fig. 2(b). So, the minima in the DOS for upper (lower) layer lies at $E = |V|/2$. This results in a finite density of states at the Fermi energy. The shift in the position of the DOS minima will have nontrivial influence on impurity states as discussed below.

The difference in the DOS of single and bilayer graphene can be studied by using finite value of t_{\perp} . In Fig. 2(c-d) we show the DOS at four sites for various values of t_{\perp} but fixed $V = 0$. The DOS at A_1, A_2 is equal and similarly DOS at B_1, B_2 is equal but those at A sites and B sites are not equal in the energy range $-t_{\perp} < E < t_{\perp}$. In this energy range, the DOS at A sites is smaller than that at B sites. In particular, at the Fermi energy, the DOS at B sites is finite but that at A sites is zero. These effects can be understood in terms of the difference in the band structure caused by finite t_{\perp} . The band structure corresponding to sites A_1

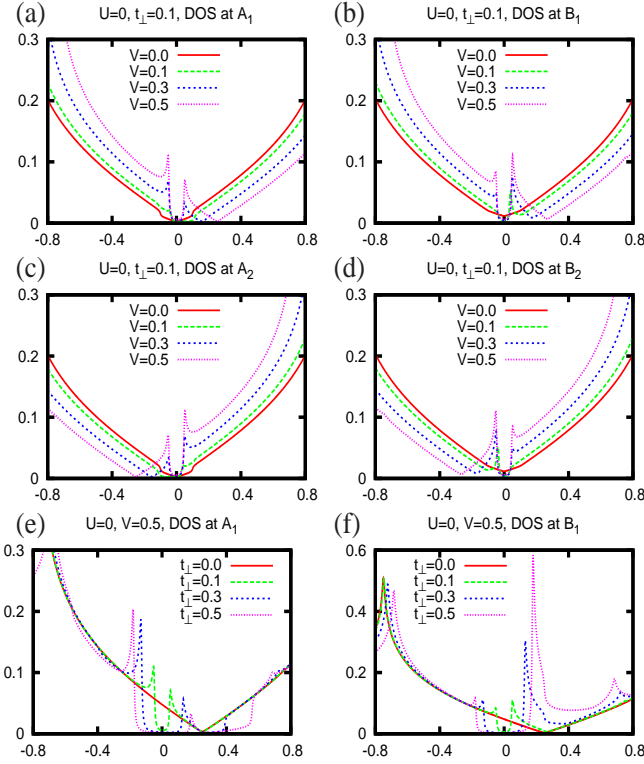


FIG. 3: (Color online) LDOS in the absence of impurity at fixed $t_{\perp} = 0.1$ and different V . The minimum of the DOS is at $|V|/2$. Small enhancement of the DOS occurs close to Fermi energy with the increase in V . We will show later that the position of this enhancement depends on t_{\perp} . There is a rearrangement of DOS between A, B sites. e) and f) LDOS at site A_1 and B_1 (respectively) at fixed $V = 0.5$ and different t_{\perp} is shown. We see gap opening around the Fermi energy. The magnitude of the gap increases with the increase in t_{\perp} . LDOS at site A_2, B_2 can be obtained by mirror inversion to the curves in Fig. 3(e) and 3(f) about the axis of $E = 0$, respectively.

and A_2 describe the anti-bonding states characterized by band gaps of $\pm t_{\perp}$ which results in the decreased density of states compared to that of the single layer graphene where corresponding bands are gapless. On the other hand, the band structure corresponding to the sites B_1 and B_2 is gapless at the Fermi energy and has more flat band compared to the single layer case resulting in finite density of states at the Fermi level. An interesting point is that the DOS at B sites is also linear even though the dispersion relation of the electron corresponding to B sites can be approximated by parabolic dispersion at low momenta.

Here, we also discuss the combined effect of bias and interlayer hopping on the DOS. In Fig. 3(a-d) we have shown the DOS at four sites for fixed $t_{\perp} = 0.1$ and different V . In Fig. 3(e-f) we have also shown the DOS at A_1 and B_1 for fixed $V = 0.5$ and different t_{\perp} . Some new features are seen in these figures. The DOS at all sites gets modified compared to the unbiased case (com-

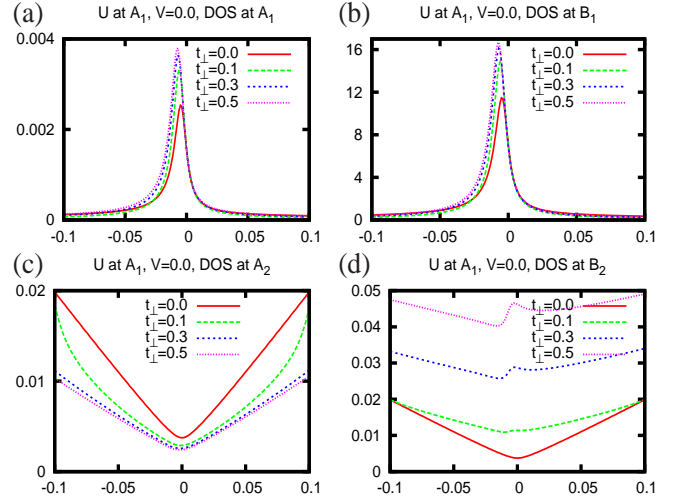


FIG. 4: (Color online) For single impurity at site A_1 DOS as a function of energy is shown. DOS at the impurity site, A_1 , is very small. DOS at the neighboring site in the same layer, B_1 , is very high which is the signature of the impurity resonance. The resonance is close to the Fermi energy. Qualitatively, the DOS at site A_2 is similar as in non impurity case, Fig. 2(c), but it changes at site B_2 . There is small oscillation in the DOS close to Fermi energy at site B_2 .

pare with Fig. 2(c) and (d)). There is a shift of DOS minimum to $E = \pm V/2$ compared to $V = 0$ case. There is also a gap opening up around the Fermi energy which increases with the increase in t_{\perp} . These unique features of band structure will lead to non-trivial impurity states.

B. Impurity states

We now discuss a single impurity in the absence of the external bias. First we put an impurity at A_1 and study the DOS for various values of t_{\perp} . The result of the actual calculation is shown in Fig. 4. The impurity has the following effects: The DOS at the impurity site, A_1 , decreases sharply. The DOS at site B_1 increases sharply which is the signature of a virtually bound impurity resonance state. The position of the resonance peak shifts slightly below the Fermi energy with the increase in t_{\perp} . This shift of the resonance peak is expected because the t_{\perp} also affects the pole of the Greens function as determined by the band structure. The width of the resonance peak decreases with t_{\perp} . This is expected because increase in t_{\perp} depresses the band DOS on site A_1 , which suppresses the scattering rate from the generated impurity state. It corresponds to an increase of lifetime, signifying a sharp resonance.

The effect on the DOS at A_2 due to the impurity at A_1 is very small. The overall behavior of the DOS curve does not change as shown in Fig. 4(c). We see a finite DOS at A_2 at the Fermi energy which is nothing but the finite size effect, which is not seen in Fig. 2(c) because of the extended scale used to show the DOS. When we

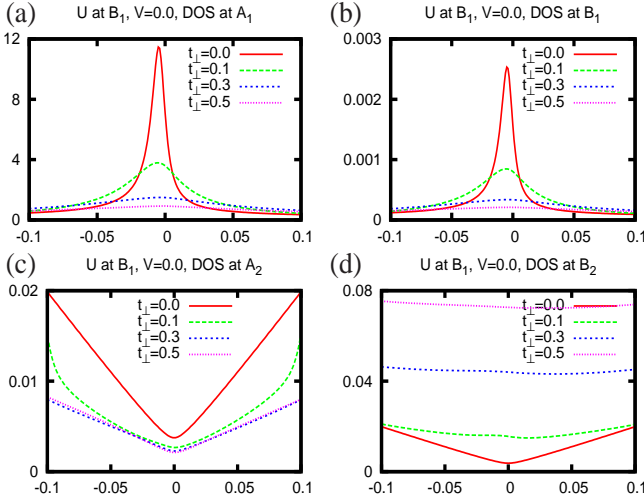


FIG. 5: (Color online) For single impurity at site B_1 , DOS as a function of energy is shown. DOS at the impurity site, B_1 , is very small. DOS at the neighboring site in the same layer, A_1 , is very high which is the signature of the impurity resonance. The resonance is close to the Fermi energy. Qualitatively, the DOS at site A_2 is similar as in non impurity case, Fig. 2c, but it changes at site B_2 . There is small oscillation in the DOS close to Fermi energy at site B_2 .

zoom in and compare Fig. 2(c) and Fig. 4(c) we see small enhancement in DOS at site A_2 in the presence of impurity at A_1 (except for $t_\perp = 0$). We see some new feature in the DOS at B_2 , namely the dip-hump structure in DOS close to the Fermi energy. We believe that the small change in the DOS at A_2, B_2 is due to the Friedel oscillation in the bottom layer created due to the impurity at the top layer. The strength of the Friedel oscillation in the bottom layer is very small because of the geometry effect.

Now we turn to discussion on the DOS when the impurity is at site B_1 , Fig. 5. We find that the DOS at site B_1 is sharply reduced. At all other sites the DOS increases compared to the clean case, which is different from the result of the single impurity at A_1 case. The DOS at A_1 increases sharply which signifies the virtual bound state due to the impurity resonance. We notice that the height of the resonance peak at site A_1 decreases with the increase in t_\perp . Simultaneously, the resonance becomes more broader. This effect is just opposite to the effect seen in the case when the impurity is at site A_1 . This effect can be understood in terms of the band structure corresponding to the site B . The increase in t_\perp enhances the band DOS on site B_1 , which increases the scattering rate from the generated impurity state. It corresponds to a decrease of lifetime, signifying a broader resonance. There is no much change in the overall behavior of the DOS at site A_2 compared to the no impurity case, Fig. 2(c). At site B_2 we see some new features, namely the dip-hump structure. Compared to the similar effect seen at B_2 due to impurity at site A_1 , the structure of DOS in the present case is weaker. It is because the effect gets

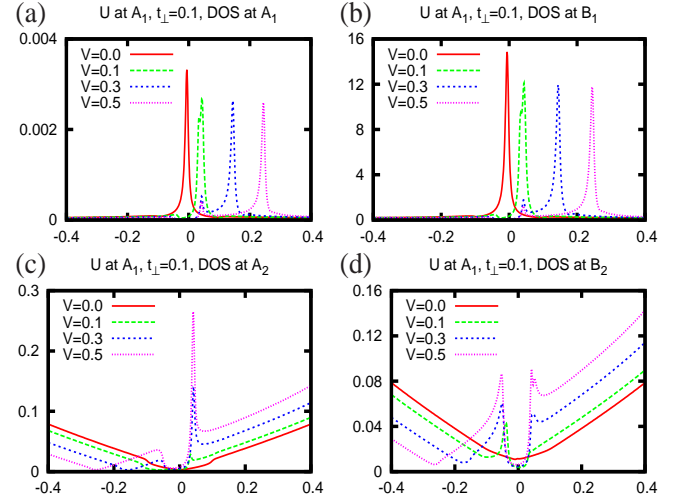


FIG. 6: (Color online) LDOS for single impurity at site A_1 with $t_\perp = 0.1$ fixed for different values of V . There is impurity resonance at site B_1 . The impurity resonance is at $E = V/2$. We also see an enhancement of the DOS at site A_2 assisted by the presence of impurity at A_1 . We also see insignificant change in DOS at site B_2 .

communicated to site B_2 through A_1 and A_2 which will be weaker than the previous case where the effect was communicated through only one bonding length.

Having discussed the effect in the single impurity case, it is much easier to understand the double impurity case. When there are two impurities at sites A_1 and A_2 , the impurity resonance occurs at site B_1 and B_2 . The DOS at B_1 and B_2 are identical. The height of the resonance peak increases with the increase in t_\perp and the resonance becomes sharper and sharper. When there are two impurities at sites B_1 and B_2 , the impurity resonance occurs at site A_1 and A_2 . The DOS at A_1 and A_2 are identical. The height of the resonance peak decreases with the increase in t_\perp and the peak width becomes broader.

Now we proceed to discuss the effect of bias on the impurity states in bilayer graphene. When there is a single impurity at site A_1 , we see impurity resonance at site B_1 , Fig. 6(b). The position of the resonance moves above the Fermi energy by $V/2$. The height of the resonance decreases slightly with the increase in the V . We also see small satellite peak near the Fermi energy. At site A_2 also we see impurity assisted enhancement in DOS on the gap edge, (compare with Fig. 3c). At site B_2 the DOS does not show much of qualitative change.

To better understand the results, especially the satellite peak of Fig. 6(b) and the position of the enhancement peak of Fig. 6(c) and (d), we study the change in LDOS due to change in t_\perp for fixed $V = 0.5$. The result is shown in Fig. 7. We find some new information from this calculation. The strength of the satellite peak, seen in DOS at B_1 , grows with t_\perp . We find that the position of the peak is determined by both V and t_\perp . The calculation shows that the position of the satellite peak is

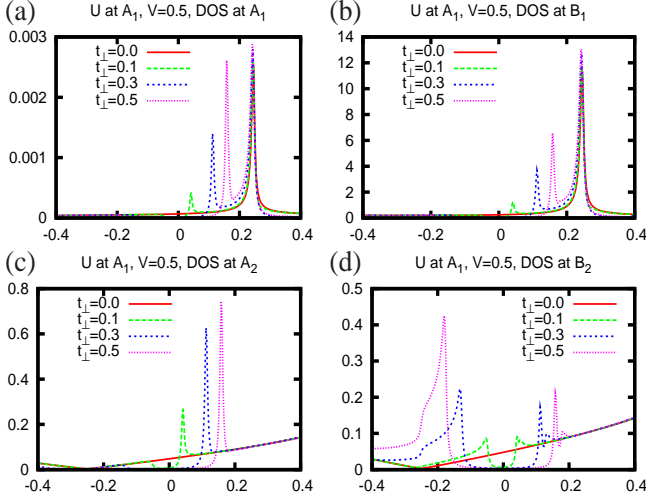


FIG. 7: (Color online) LDOS for a single impurity at site A_1 , for $V = 0.5$ fixed, and with the variation in t_\perp .

at $E_g = \frac{V}{2} \left[\frac{t_\perp^2}{t_\perp^2 + V^2} \right]^2$. This is equal to the energy gap of the second dip in the dispersion relation of the bilayer graphene in the presence of the external bias. The edge of the band gap seen in Fig. 3 is also at $E = E_g$. Similar behavior is seen at site A_2 . The enhancement of the DOS seen in Fig. 6(c) for $V = 0.5$ increases with t_\perp . The position of the peak also moves away from the Fermi energy by E_g . At site B_2 new features are seen. The height of the small satellite peak increases with t_\perp . The position of the peak also shifts symmetrically above and below the Fermi level by E_g . With the increase in t_\perp a clear sign of the gap opening is seen around the Fermi energy.

When there is a single impurity at site B_1 (see Fig. 8), we see different features than when there is an impurity at A_1 . At $V = 0$ there is a single impurity resonance close to the Fermi energy. When there is an external bias, the resonance peak at site A_1 splits in two peaks. One of the peak lies at $E = V/2$ above the Fermi energy. Other remains close to the Fermi energy. With the increase in V , the intensity of the peak at $V/2$ increases and that close to the Fermi energy decreases. At site A_2 and B_2 we see impurity assisted enhanced DOS close to the Fermi energy.

To better understand the result presented in Fig. 8 we perform another calculation for LDOS at fixed $V = 0.5$ and different t_\perp . The result is shown in Fig. 9. In the Fig. 9(a) we can see that the weight of LDOS at $E = V/2$ decreases with t_\perp . This loss of weight is transferred close to the Fermi energy. This phenomenon can be understood in terms of the change in LDOS (at fixed $V = 0.5$ in the absence of the impurity) due to the change in t_\perp , (see Fig. 3(e), and 3f)), where we see that finite t_\perp opens up a gap around the Fermi energy and the gap becomes more and more well defined for increased t_\perp . This gap leads to a new resonance state around the Fermi energy in the presence of the impurity. The shift of the weight

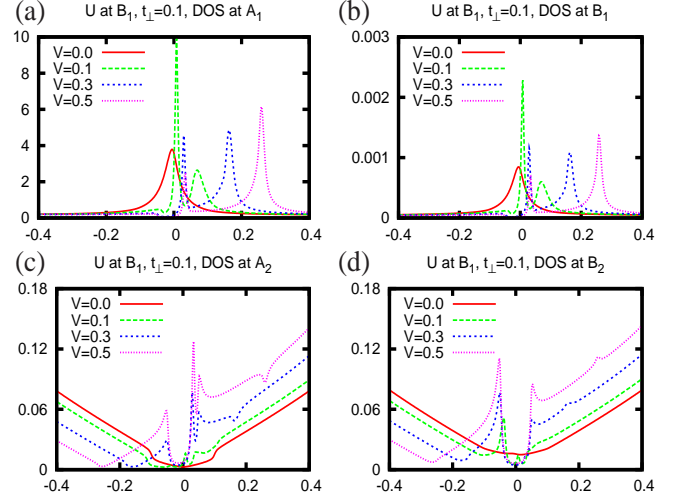


FIG. 8: (Color online) In addition to a resonance which follows $V/2$, we see some interesting features at sites A_2 , B_2 .

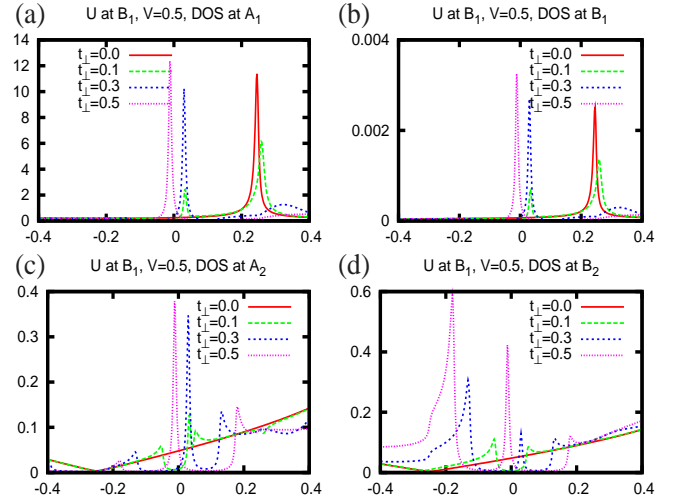


FIG. 9: (Color online) LDOS for a single impurity at site B_1 , for $V = 0.5$, and with the variation in t_\perp .

of the LDOS close to the Fermi energy at site A_2 and B_2 , can also be understood using the same logic. We can also see in Fig. 3(f) that the LDOS at site B_1 at $E = V/2$ increases with the increase in t_\perp which explains the broadening effect seen in Fig. 9(a) near $E = V/2$.

When we have two impurities at A_1 and A_2 we see impurity resonances at B_1 and B_2 . The position of the impurity resonance is again determined by $V/2$. Interestingly, the impurity resonance at site B_1 lies above the Fermi energy whereas that at site B_2 is below the Fermi energy. The DOS at B_1 can be obtained by mirror reflection of the DOS at B_2 about the axis of $E = 0$.

When we put two impurities at B_1 and B_2 impurity resonance arises at A_1 and A_2 . The position of the impurity resonance is again determined by $V/2$. The impurity resonance at site A_1 lies above the Fermi energy whereas that at site A_2 is below the Fermi energy. The DOS at

A_1 can be obtained by mirror reflection of the DOS at A_2 about the axis of $E = 0$.

IV. CONCLUDING REMARKS

Before concluding, we would like to make two comments. To our knowledge two studies have been done which resembles to our work. Wang et. al.¹² have studied the effects of voids in the absence of external bias. In particular they investigated the quantum interference pattern in a specific energy and no impurity induced resonance states were discussed. Similarly, the disorder problem in biased bilayer graphene was studied by Nilsson and Castro Neto.⁹ In our work we have addressed the issue about the sensitivity of the impurity induced resonance states to the underlying electronic band structure in a bilayer graphene, through the application of pressure

or/and electric bias, which were not touched in these literatures.

In conclusion we study the possibility of tuning impurity states in a bilayer graphene. We systematically study the signature of the impurity resonance states by looking at the local density of states at four inequivalent sites of the bilayer graphene. This work should be the most detailed study of the impurity states in bilayer graphene. We have shown that in bilayer graphene the impurity states can be tuned using an external bias and changing the interlayer hopping energy. Our predictions about the evolution of the impurity states in bilayer graphene can be tested by the scanning tunnelling microscopy.

Acknowledgements: One of us (H.D.) is grateful to K. Bedell and the Boston College for financial support. This work was supported by DOE at Los Alamos under Grant No. DE-AC52-06NA25396 and the LDRD programs.

* Electronic address: jxzh@lanl.gov;
URL: <http://theory.lanl.gov>

¹ K. S. Novoselov, V. V. K. D. Jiang, T. Booth, S. M. Morozov, and A. K. Geim, Proc. Natl. Acad. Sci. U.S.A. **102**, 10451 (2005).

² K. S. Novoselov, A. K. Geim, S. V. Morozov, D. Jiang, M. I. Katsnelson, I. V. Grigorieva, S. V. Dubonos, and A. A. Firsov, Nature **438**, 197 (2005).

³ K. S. Novoselov, E. McCann, S. V. Morozov, V. I. Falko, M. I. Katsnelson, U. Zeitler, D. Jiang, F. Schedin, and A. K. Geim, Nature Physics **2**, 177 (2006).

⁴ P. R. Wallace, Phys. Rev. **71**, 622 (1947).

⁵ J. Nilsson, A. H. Neto, F. Guinea, and N. M. Peres, Phys. Rev. Lett. **97**, 266801 (2006).

⁶ J. Nilsson, A. H. Castro Neto, F. Guinea, and N. M. R. Peres, Phys. Rev. Lett. **97**, 266801 (2006).

⁷ E. McCann and V. I. Falko, Phys. Rev. Lett. **96**, 086805 (2006).

⁸ E. McCann, Phys. Rev. B **74**, 161403 (2006).

⁹ J. Nilsson and A. H. Castro Neto, Phys. Rev. Lett. **98**, 126801 (2007).

¹⁰ T. O. Wehling, A. V. Balatsky, M. I. Katsnelson, A. I. Lichtenstein, K. Scharnberg, and R. Wiesendanger, Phys. Rev. B **75**, 125425 (2007).

¹¹ C. Bena, cond-matt/0706411 (2007).

¹² Z. F. Wang, Q. Li, H. Su, X. Wang, Q. W. Shi, J. Yang, and J. G. Hou, Phys. Rev. B **75**, 085424 (2007).